

Radio-loudness statistics of quasars from Quiaia–VLASS

N. Arsenov^{1,2}, S. Frey^{3,4,5}, A. Kovács^{2,3,4}, and L. Slavcheva-Mihova¹

¹ Institute of Astronomy and NAO, Bulgarian Academy of Sciences, 72 Tsarigradsko Chaussee Blvd., 1784 Sofia, Bulgaria
e-mail: narsenov@astro.bas.bg

² MTA–CSFK *Lendület* “Momentum” Large-Scale Structure (LSS) Research Group, Konkoly Thege Miklós út 15-17, H-1121 Budapest, Hungary

³ Konkoly Observatory, HUN-REN Research Centre for Astronomy and Earth Sciences, Konkoly Thege Miklós út 15-17, H-1121 Budapest, Hungary

⁴ CSFK, MTA Centre of Excellence, Konkoly Thege Miklós út 15-17, H-1121 Budapest, Hungary

⁵ Institute of Physics and Astronomy, ELTE Eötvös Loránd University, Pázmány Péter sétány 1/A, H-1117 Budapest, Hungary

Received November 2024

ABSTRACT

Context. Quasars are objects of high interest for applications in extragalactic astrophysics, cosmology, and astrometry. One of their useful qualities is owed to their relativistic jets: they can be radio-loud. However, the fraction of radio-loud vs. radio-quiet quasars is subject to ongoing investigations, where the statistical power is limited by the low number of known quasars with radio counterparts.

Aims. In this analysis, we revisited the radio-loudness statistics of quasars by significantly expanding the pool of known sources. Our main goal was to create a new, value-added catalogue of quasars with information about their extinction-corrected magnitudes, radio flux density, possible contamination levels, and other data flags, besides their sky coordinates and photometric redshifts.

Methods. We cross-matched the optical *Quiaia* catalogue of about 1.3 million quasars (selected from the *Gaia* data set) with 1.9 million sources from the Very Large Array Sky Survey (VLASS) radio catalogue. We explored different thresholds for the matching radius, balancing the completeness and purity of the resulting *Quiaia*–VLASS catalogue, and found that 1.5" is a sufficient choice.

Results. Our main finding is that the radio-loud fraction of quasars is in good agreement with previous works (< 10%), and there is no significant large-scale pattern in radio-loudness across the sky. The exact estimate depends on the *G*-band magnitude limit, and we observed some weak trends with redshift and absolute optical magnitude, possibly indicating remnant systematic effects in our data sets. The cross-matched *Quiaia*–VLASS catalogue with 43,650 sources is available to the public for future analyses.

Conclusions. This latest census of QSOs with radio counterparts will facilitate further investigations of the dichotomy of radio-loud and radio-quiet quasars, and it may also support other lines of statistical investigations using quasars in cosmology and astrophysics.

Key words. catalogs – surveys – galaxies: active – quasars: general – radio continuum: galaxies – large-scale structure of Universe

1. Introduction

Active galactic nuclei (AGN) are among the most powerful and dynamic objects in the Universe (e.g. [Padovani et al. 2017](#)), usually outshining their host galaxies. They can be found over a wide range of distances from the local Universe up to extremely high redshifts ($z \gtrsim 10$, [Goulding et al. 2023](#)). AGN play an important role in astrophysics, astrometry, and cosmology. They are located at the centres of galaxies and powered by accretion onto supermassive black holes (SMBHs) which range from millions to billions of solar masses. As material spirals into the SMBH, it heats up and emits huge amounts of energy across the entire electromagnetic spectrum, from radio to γ -rays.

Members of a small but spectacular subset of AGN exhibit intense radio emission originating from synchrotron radiation of relativistic charged particles moving in magnetized plasma jets launched from the close vicinity of SMBHs (e.g. [Urry & Padovani 1995](#); [Blandford et al. 2019](#)). Studying these so-called radio-loud, or rather jetted ([Padovani 2017](#)) AGN is crucial for several reasons. Their jets are among the most extreme particle accelerators in the Universe, giving unique insight into relativistic effects, strong magnetic fields, and high-energy particle interactions. The radiative and mechanical feedback of AGN jets can influence the evolution of their host galaxies by regulating star formation (e.g. [Fabian 2012](#); [Hardcastle & Croston 2020](#)).

Owing to their presence in the widest range of cosmological distances, AGN are excellent probes of the early Universe and offer the possibility of contributing to the studies of cosmological models (e.g. [Vermeulen & Cohen 1994](#); [Gurvits et al. 1999](#)). AGN also trace cosmic structures and thus are important for understanding the large-scale distribution of matter (see e.g. [Kovács et al. 2022](#); [Piccirilli et al. 2024](#)). In astrometry, bright radio-emitting AGN define the most precise reference frame through high-resolution very long baseline interferometry (VLBI) observations ([Charlot et al. 2020](#)).

A subclass of AGN, quasars (originally meaning quasi-stellar radio sources) were discovered as distant extragalactic objects in the early 1960's ([Schmidt 1963](#)). Not much later, it turned out that the majority of the so-called quasi-stellar objects (QSOs, also called quasars for simplicity) are not strong radio emitters ([Sandage 1965](#)). Nowadays, the number of known quasars with measured spectroscopic redshifts exceeds 1 million ([Flesch 2023](#)). The fraction of radio-loud quasars among the whole population is known to be $\lesssim 10\%$ (e.g. [Ivezić et al. 2002](#); [Kellermann et al. 2016](#)).

There are various working definitions of radio loudness in the literature. One can use the radio-to-optical flux density ratios as originally proposed by [Schmidt \(1970\)](#). Perhaps the most widely used definition is based on the ratio of the rest-frame 5-

Quaia QSO catalog, limited to Dec > -40°

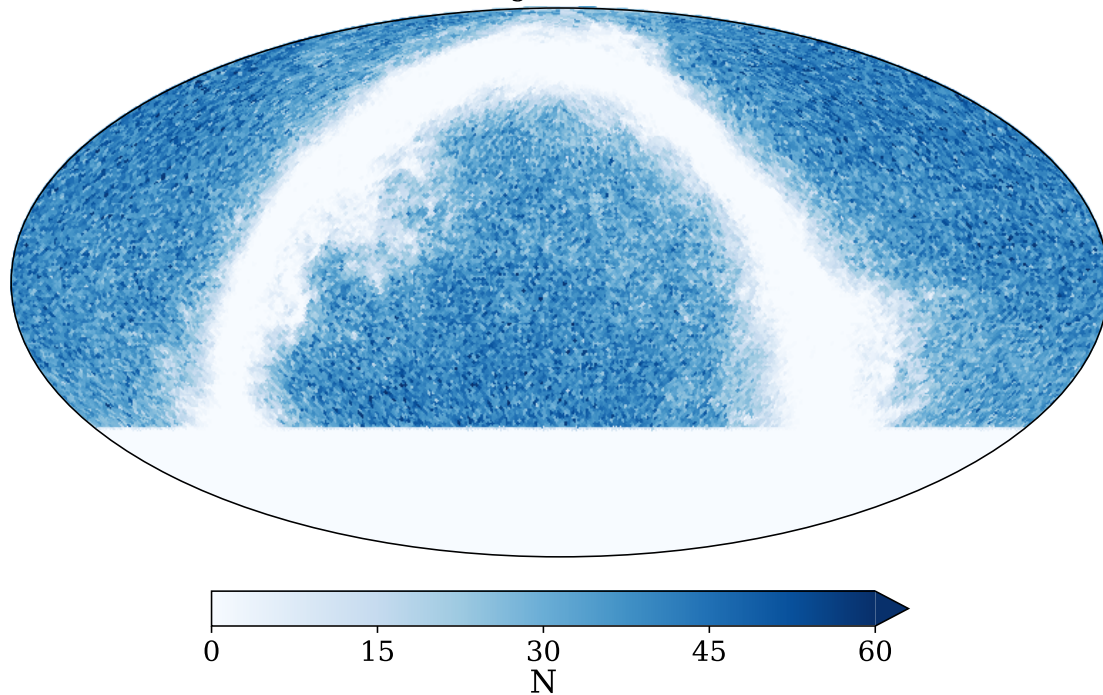


Fig. 1: The distribution of the 1.1 million *Quaia* sources that fall within the joint coverage with the VLASS survey ($\delta > -40^\circ$). The dust obscuration in the Milky Way disc results in the detection of fewer QSOs in the optical.

GHz radio and 4400-Å optical flux densities (Kellermann et al. 1989). If this ratio R exceeds 10 then the object is considered radio-loud. Sramek & Weedman (1980) used 2500-Å optical flux densities. Given the well-known flux density variability of quasars and the fact that optical and radio measurements are rarely contemporaneous, R values themselves can be uncertain.

The above two definitions are broadly consistent with each other for the quasar class as a whole (see a recent example in Krezinger et al. 2024). Alternatively, dictated by practical aspects such as the availability of measurements, it is customary to use other radio and optical bands, e.g. 1.4 GHz in the radio and the i -band in the optical (like in Ivezić et al. 2002; Baloković et al. 2012). Note that Terashima & Wilson (2003) defined radio loudness as the ratio of radio (5 GHz) and X-ray (2 – 10 keV band) luminosities that can be applied for heavily obscured AGN. A fundamentally different approach is defining radio loudness by setting a threshold based on the (monochromatic) radio luminosity (e.g. Peacock et al. 1986; Miller et al. 1990). Interestingly, the two types of definitions provide generally similar classifications, as discussed in Appendix C of Ivezić et al. (2002).

The ‘classical’ definition of radio loudness based on radio and optical flux density ratios is the best applicable for quasars where the optical emission is dominantly related to the accretion disk while the radio emission comes mainly from the jets (Padovani 2017). Most early publications found a bimodal distribution of radio-loud and radio-quiet (in fact, not totally free from radio emission, rather radio-weak) quasars (e.g. Strittmatter et al. 1980; Kellermann et al. 1989; Miller et al. 1990; Ivezić et al. 2002). While the debate about this dichotomy is not settled yet, a consensus seems to emerge that radio loudness has a continuous distribution with no sharp gap between radio-loud and radio-quiet sources (see a review in Kellermann et al. 2016).

For a long time, studies of radio loudness were naturally limited to small samples of relatively bright AGN. The emergence of sensitive large radio and optical sky surveys (e.g. Ivezić et al. 2002; Gürkan et al. 2019; Arnaudova et al. 2024) made substantially larger samples available for investigations. Here we revisit the problem with modern optical and radio surveys, and perform various statistical tests of radio-loudness of quasars.

The paper is organized as follows. In Sect. 2, we introduce our observational data sets and the analysis methodology. Then, Sect. 3 contains our observational results, followed by a summary of our main conclusions in Sect. 4.

2. Data sets and methodology

The main goal of this work is to cross-match a large sample of optically detected quasars with a catalogue of radio sources, mainly following the footsteps of Ivezić et al. (2002), concentrating on the radio-loudness statistics. In this section, we present the input data sets and the technical details of the cross-matching process.

For the optical quasar catalogue, we chose the recently compiled *Quaia* (Storey-Fisher et al. 2024) because of its large sky coverage, high completeness, and high astrometric accuracy. For the radio data, we relied on the Very Large Array Sky Survey (VLASS, Lacy et al. 2020) which is superior to all previous large sky surveys in terms of positional accuracy, angular resolution, and sensitivity.

2.1. Quasar catalogue

For our cross-matched sample, we used the *Quaia* quasar catalogue (Storey-Fisher et al. 2024), culled from the *Gaia* space telescope’s data set (Gaia Collaboration et al. 2016). The QSOs

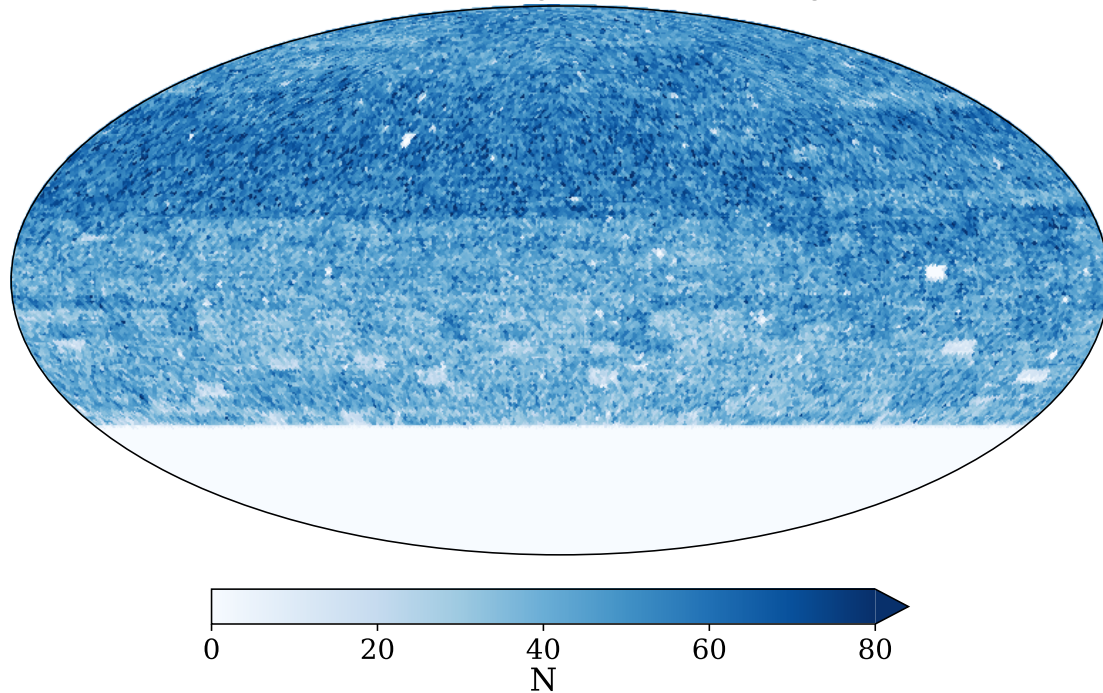
VLASS, Quick Look catalog, epoch 2, $v=2$, flags applied

Fig. 2: The distribution of the 1.9 million VLASS2 QL sources after applying quality flags (see Table 1). Unlike for optical QSOs, the radio coverage is virtually unaffected by the Galactic disc.

of the *Quaia* catalogue are distinguished from the other types of sources by cross-matching the *Gaia* Data Release 3 (DR3) QSO candidates (Gaia Collaboration et al. 2023b,a; Delchambre et al. 2023) with infrared sources from the *Wide-field Infrared Survey Explorer* (WISE, Lang 2014), applying colour cuts within the *Gaia*–WISE photometry parameter space and cutting out sources with high proper motions.

More precisely, we used the *Quaia* catalogue restricted in magnitude to $G < 20.5$, containing about 1.3 million QSOs, which yields high completeness of quasars within the *Gaia* sky coverage. There is also a conservative *Quaia* catalogue, a subsample of the larger one, with a constraint of $G < 20.0$, with the benefit of the latter constraint yielding a purer QSO sample with a higher fidelity of the sources being QSOs. We decided to use the more complete catalogue with $G < 20.5$, because its contaminants are expected to be mostly stars and should have negligible emission in the radio.

Another *Quaia* data product that we used is the so-called selection function, which indicates the QSO completeness due to various systematic effects (see Storey-Fisher et al. 2024, for details). The sky coverage of the *Quaia* catalogue that we consider in this analysis is displayed in Fig. 1.

2.2. Radio sources

The other data set that we used is based on the ongoing VLASS (Lacy et al. 2020) at 3 GHz (S-band), conducted with the Very Large Array in New Mexico, in particular the VLASS Epoch 2 Quick Look (VLASS2 QL) catalogue. Unlike *Quaia*, the VLASS2 QL catalogue does not cover the full sky, and its 3.0 million radio sources are distributed at declinations $\delta > -40^\circ$.

Further, VLASS is conducted in a single band, making it more difficult to deduce the class of the detected objects than

for optical surveys with multiple bands, e.g. by segmentation in colour–colour space. Hence, cross-matching VLASS with another large-scale catalogue like *Quaia* is a straightforward choice for sampling radio-loud extragalactic objects. The sky area density of the VLASS2 QL catalogue, with applied quality flags, is displayed in Fig. 2.

For our purposes, we applied the VLASS data flags explicitly recommended by the user manual (Gordon et al. 2023) to restrict ourselves to the most reliable data. We used the VLASS catalogue flag setting *Duplicate_flag* < 2 to get rid of any duplicated radio sources, originating from overlaps of the sky patches observed in the survey.

Further, we only used VLASS sources with *Quality_flag* == 0 (no quality issues) and $(Quality_flag == 4) \& (S_Code \neq 'E')$ (integrated flux density is less than the peak brightness, but everything else in the measurement is acceptable). Table 1 shows the number of sources within the input data sets, after the quality cuts and the different G magnitude bins that we used.

2.3. Cross-matching

In order to create a cross-matched sample, we determined the common, physically identical sources within *Quaia* and VLASS. We first identified for each *Quaia* source its closest counterpart in VLASS and then calculated the corresponding angular separation between their sky coordinates ($\Delta\theta$). This method has been previously used, among others, by Ivezić et al. (2002); Orosz & Frey (2013).

Next, we determined an optimal angular separation threshold $\Delta\theta_t$, for which one can safely assume that sources with $\Delta\theta < \Delta\theta_t$ are physically related in *Quaia* and VLASS, while sources with $\Delta\theta \geq \Delta\theta_t$ are plausibly just chance alignments of non-identical sources. An optimal choice of $\Delta\theta_t$ should be large enough to al-

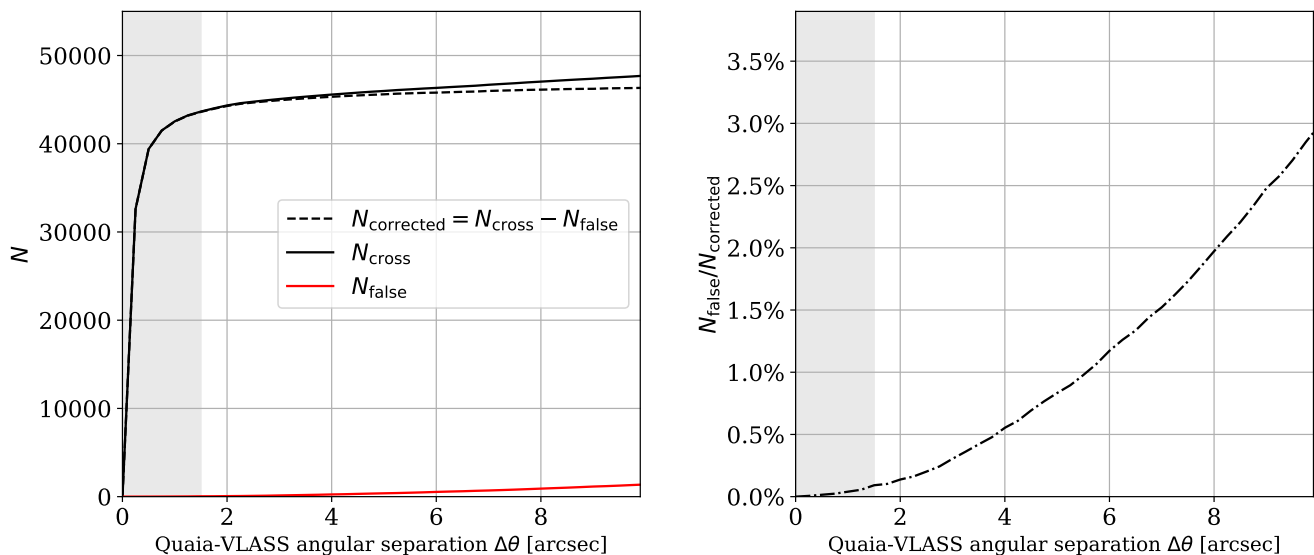


Fig. 3: *Left:* the number of cross-matched sources as a function of a search radius parameter in arcseconds. We performed a robustness test using randomly perturbed sky coordinates, and found that a search radius of $1.5''$ results in a low level of contamination ($< 0.1\%$) from false matches (*right*). We thus choose this threshold for our cross-matched *Quaia*–VLASS sample.

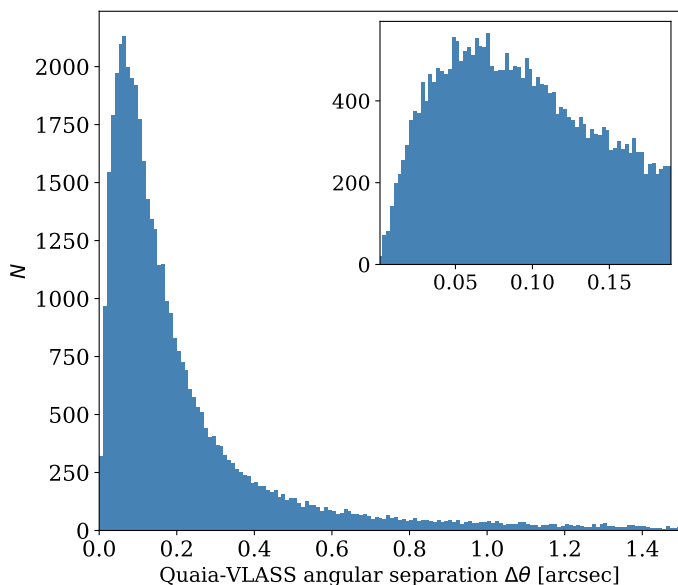


Fig. 4: The distribution of angular separation values when cross-matching the *Quaia* and VLASS samples, up to the $1.5''$ search radius threshold that we applied. The inset shows the closest matches below $\Delta\theta = 0.2''$.

low for a large number of proper physical cross-matches to be identified as such (high completeness of the sample). Simultaneously, $\Delta\theta_t$ should be reasonably small to prevent contamination of the cross-matched population with chance-aligned sources (high-purity sample).

In Fig. 3, we present our findings in the context of the fraction of possibly false matches. In the left panel, N_{cross} is the cumulative number of cross-matches between *Quaia* and VLASS as a function of the coordinate separation up to the corresponding $\Delta\theta$ value. We also display N_{false} , calculated with a method used previously by Orosz & Frey (2013). N_{false} measures a cross-matched fraction between VLASS and *Quaia*^{*}, where *Quaia*^{*} is a surrogate of the *Quaia* QSO catalogue with all sources rotated

Table 1: Population statistics for the different data sets used.

Source catalogues	N_{sources}	Radio-loud
<i>Quaia</i> , full ($G < 20.5$)	1,295,502	-
<i>Quaia</i> , $\delta > -40^\circ$ cut	1,084,545	-
VLASS2 QL	2,995,025	-
VLASS2 QL, flags applied	1,873,524	-
<i>Quaia</i> –VLASS (all)	43,650	$3.83\% \pm 0.02\%$
$14.0 < G < 18.5$ cut	9,395	$8.04\% \pm 0.09\%$
$18.5 \leq G < 19.5$ cut	15,763	$4.71\% \pm 0.04\%$
$19.5 \leq G < 20.5$ cut	18,492	$2.80\% \pm 0.02\%$

Notes. *Top:* the number of sources contained in the data sets that we used. *Bottom:* The radio-loud fraction of sources in the full *Quaia*–VLASS cross-match and in subsets due to different cuts in G optical magnitude (errors are based on Poisson statistics).

randomly by the same angle in right ascension. This ensures that N_{false} from cross-matching *Quaia*^{*} and VLASS only contains unphysical chance alignments. Moreover, N_{false} should approximate the chance alignments between *Quaia* and VLASS very well, because *Quaia*^{*} has the same source density as *Quaia*. The curve of $N_{\text{corrected}} = N_{\text{cross}} - N_{\text{false}}$ demonstrates a saturation in the number of physical cross-matches at $\Delta\theta \approx 1.5''$ (displayed as a grey band).

Using the above estimate of the contamination, in Fig. 3 (right panel) we show the fraction of chance alignments as a function of $\Delta\theta$, which can be expressed as

$$f(\theta) = \frac{N_{\text{false}}(\theta)}{N_{\text{corrected}}(\theta)} = \frac{N_{\text{false}}(\theta)}{N_{\text{cross}}(\theta) - N_{\text{false}}(\theta)}. \quad (1)$$

At $\Delta\theta \approx 1.5''$, we estimated $N_{\text{false}}/N_{\text{corrected}} \approx 0.1\%$ contamination, i.e. excellent purity. We thus decided to apply this $\Delta\theta_t < 1.5''$ threshold for our cross-matching procedure. We note that Ivezić et al. (2002) also used the same threshold for their analysis, which makes comparisons more straightforward.

Figure 4 shows a histogram of the *Quaia*–VLASS angular separations up to $\Delta\theta = 1.5''$, indicating that most cross-matches

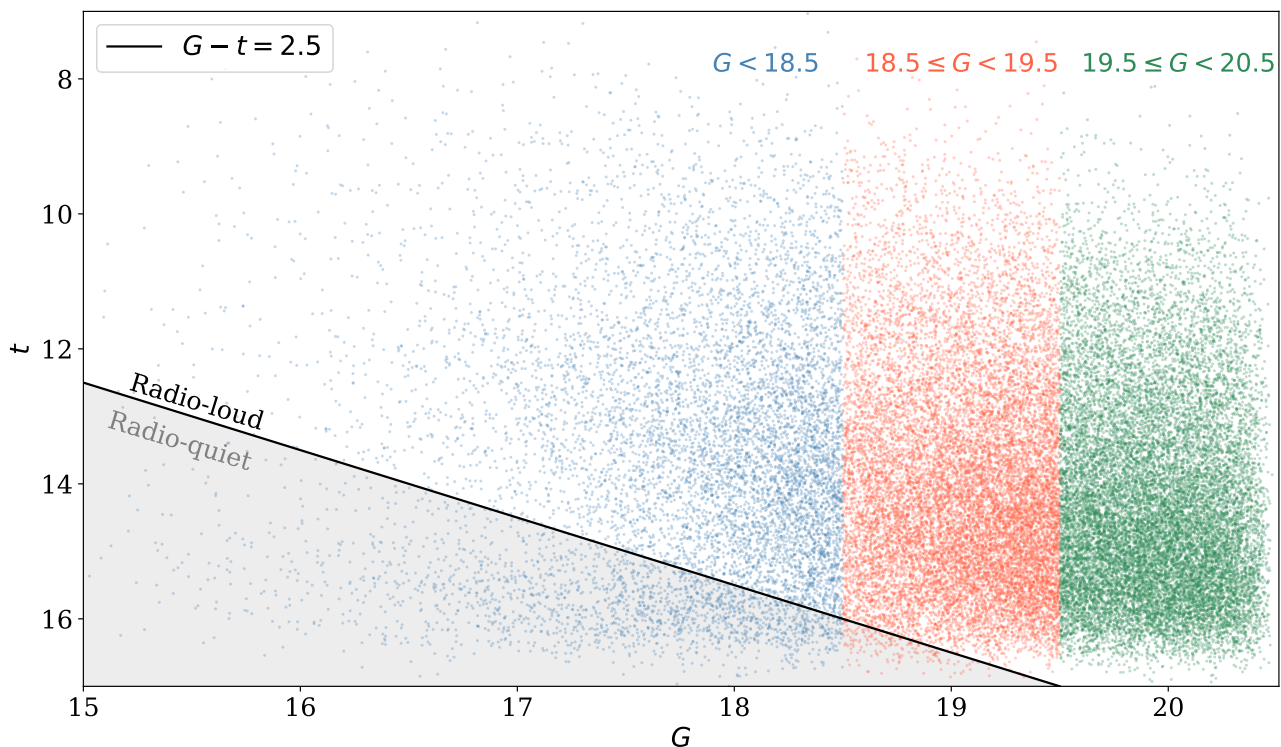


Fig. 5: The extent of our *Quaia*–VLASS sample along the G (optical) and t (radio) bands. Radio-loud and radio-quiet sources are separated by the black line. We defined three bins in the G band, which we later analyse separately in the rest of the paper when looking for brightness-dependent trends in radio loudness.

are identified with $\Delta\theta < 0.5''$ separation, with a peak at about $\Delta\theta \approx 0.07''$ (see inset of Fig. 4). We thus conclude that the construction of our cross-matched sample guarantees high completeness.

2.4. Reddening correction

As provided by Storey-Fisher et al. (2024), the G -band magnitudes of the *Quaia* sources are not corrected for Galactic extinction. We thus corrected the G -band data following the formula

$$G = G' - r \cdot \langle R_{\zeta} \rangle, \quad (2)$$

where G' is the uncorrected magnitude, G is extinction-corrected magnitude, and r is the reddening in the given region of the sky as provided by Schlegel et al. (1998). Further, $\langle R_{\zeta} \rangle \approx 2.74$ is the extinction coefficient for the *Gaia* G -band as provided by Casagrande & Vandenberg (2018). Except stated otherwise, all subsequent references in this paper to the G -band magnitude refer to the corrected value from Eq. 2.

3. Results

Using the cross-matched *Quaia*–VLASS sources, we estimated the radio loudness of our sample in various subsets and using different cuts. We used the definition by Ivezić et al. (2002) for the radio magnitude t as

$$t = -2.5 \log \left(\frac{F_{\text{tot}}}{3631 \text{Jy}} \right), \quad (3)$$

Table 2: Differences between our work and Ivezić et al. (2002).

Present work	Previous work
<i>Quaia</i> –VLASS	SDSS–FIRST
G -band + S -band	i -band + L -band
43,650 cross-matches	3066 cross-matches

where F_{tot} is the total flux density of the source (in the S -band). In Fig. 5, all the cross-matched *Quaia*–VLASS sources are displayed in a $G - t$ diagram, including a binning along the G axis for future tests. Again following Ivezić et al. (2002), we used the $G - t$ magnitude difference as a measure for the radio loudness of the sources. We defined the following two cases:

$$\begin{aligned} G - t > 2.5 &: \text{radio-loud sources} \\ G - t \leq 2.5 &: \text{radio-quiet sources} \end{aligned} \quad (4)$$

This definition was derived from the equivalent calculation in Ivezić et al. (2002), $R_m = 0.4(m - t)$, where m is a magnitude in the optical, t is the radio magnitude at 1.4 GHz (in that example, $R_m > 1$ corresponds to radio-loud and $R_m \leq 1$ to radio-quiet objects).

3.1. A high-purity catalogue of radio-loud quasars

In Fig. 5, a solid line depicts the border between radio-loud and radio-quiet sources, as expressed in Eq. 4. Sources are coloured according to bins in G , which correspond to optically bright, moderate, and faint bins (the number of sources within different G -bins is given in Table 1).

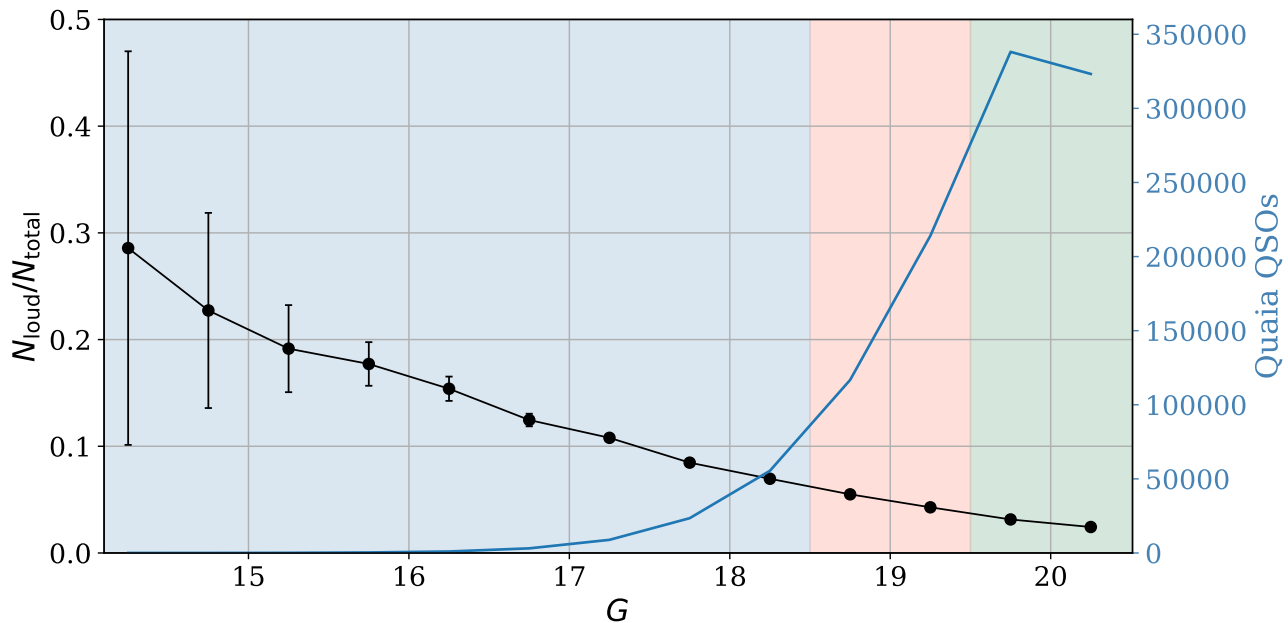


Fig. 6: The radio-loud fraction $N_{\text{loud}}/N_{\text{total}}$ of QSOs in different bins as a function of G (black curve) and the number N_{total} of *Quiaia* quasars in these bins (blue curve). The colour-coding along G is equivalent to the colour-coding in Fig. 5. The black curve shows that even though it is expected to underestimate the radio-loud fraction at $G > 18.5$, such a trend of a sudden drop in the curve is not observed.

The choice of G -band range values for these bins is motivated by a desire to keep these splits simple, yet offering meaningful comparisons to Ivezic et al. (2002). We note that while we kept t and radio loudness consistent for the sake of comparison, there are some inevitable technical differences as displayed in Table 2. The main addition is a significantly larger sky coverage, a larger cross-matched sample, and thus a reduction of possible biases in the analysis.

While the actual definitions of radio loudness may differ (as well as their range of validity), we note that of the 43,650 cross-matched *Quiaia*-VLASS quasars shown in Fig. 5 the vast majority is clearly visible in the radio (41,496 of them are radio-loud, given our definition). Therefore, an important outcome of our work is a *high-purity* catalogue of quasars with radio counterparts, which may be used in various other projects in the future.

Considering the *completeness* of our radio-loud catalogue (besides its purity), one should also consider the sensitivity limits of the input optical and radio data sets, that may bias the radio-loudness statistics for faint sources. We provide various tests of these systematic effects in the following sections, applying different binning schemes and cuts to the *Quiaia*-VLASS sample to estimate possible variations in the radio-loud fraction.

3.2. Radio-loud fraction vs. G magnitude

When estimating the radio-loud fraction ($N_{\text{loud}}/N_{\text{total}}$) of *Quiaia*-VLASS sources, it is reasonable to restrict the sample to a range where the sensitivity of the instruments is reliable, i.e. where the measured N_{loud} and N_{total} source counts are complete within a chosen magnitude limit.

Ivezic et al. (2002) applied such a restriction in the form of a cut in the optical i -band, providing a fiducial value for the fraction of radio-loud QSOs with $i < 18.5$. This particular cut follows from their radio-loudness formula ($G - t > 2.5$) and the sensitivity limit they work with in the radio ($t < 16.0$, that is

slightly more conservative than the nominal $t < 16.5$ where they still find radio sources).

In our work, we used the same Eq. 4 for defining radio loudness, and the VLASS has a similar sensitivity limit in t (see Fig. 5). While this condition motivates a cut in the *Quiaia* data at $G < 18.5$, we tested the whole $G < 20.5$ magnitude range to measure $N_{\text{loud}}/N_{\text{total}}$ for a comprehensive analysis.

Figure 5 depicts the origin of this unreliability. For fainter *Quiaia* magnitudes, the radio magnitudes may fall outside of the sensitivity limit $t \approx 16.0$, which suggests lower and lower completeness when one intends to estimate the radio-loud fraction on the faint end (while the purity of the sample is expected to remain high, as we argued above).

In Fig. 6, we show how the radio-loud fraction of QSOs drops for fainter optical sources (which are naturally more abundant in the sample). We made the following observations:

- The black line represents the radio-loud fraction of sources as a function of the G magnitude, showing a linear drop in the radio-loudness fraction.
- Also, we observed that the radio-loud fraction is not constant even in the range of the brightest sources (e.g. $G < 17$), where high completeness is expected in both N_{loud} and N_{total} .
- Further, constraining the measurement of the radio-loud fraction to $G < 18.5$ would ignore the bulk of the *Quiaia* QSOs (see the blue curve in 6) and the majority of the cross-matched sources (see Table 1).

For the above three reasons, we decided to express the radio-loud fraction of the *Quiaia*-VLASS sources as a function of G up to $G = 20.5$, and let future users of our catalogue decide how they wish to balance purity and completeness.

Nevertheless, if we apply the measure for the radio-loud fraction by Ivezic et al. (2002), then we arrive at a value of $N_{\text{loud}}/N_{\text{total}} \approx 8.04\% \pm 0.09\%$ radio-loud fraction for $G < 18.5$, while they estimate $N_{\text{loud}}/N_{\text{total}} \approx 8\% \pm 1\%$ for a similarly bright,

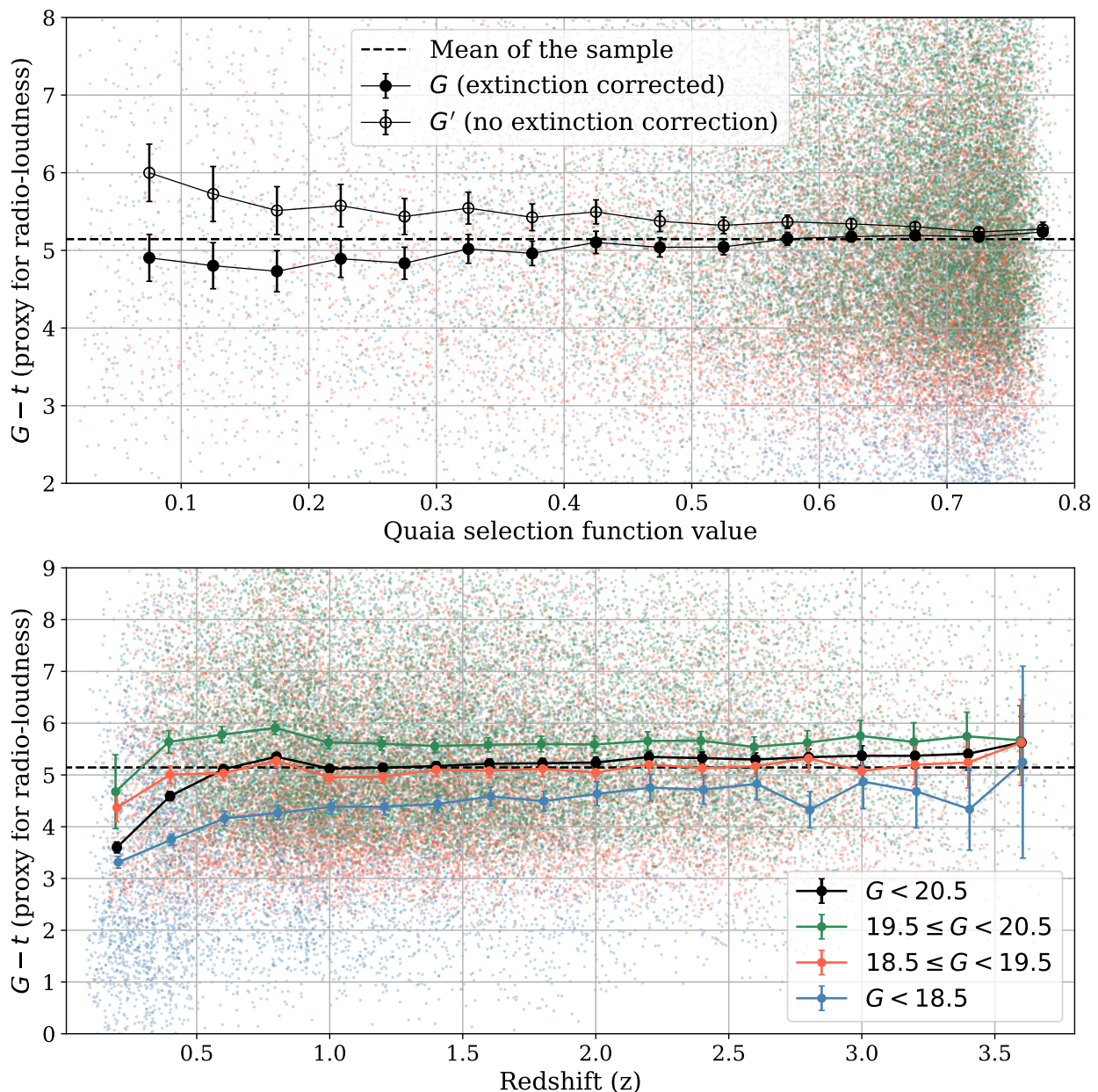


Fig. 7: The $G - t$ magnitude difference, i.e. our proxy for radio loudness, is averaged in various bins. *Top:* we bin our catalogue on the *Quaia* selection function (completeness) values, and also illustrate the role of the Galactic extinction correction. *Bottom:* we bin our sample on redshift, and also on G magnitudes (see colours), and identify weak trends at the lowest redshifts ($z < 0.5$).

conservatively selected subset of their data ($i < 18.5$). Again, we note the differences between the actual bands used by Ivezić et al. (2002) and our analysis, but we conclude that consistent radio-loud fraction values are observed for the brightest QSOs.

3.3. Radio loudness vs. QSO completeness

In Fig. 7, we show multiple tests that we performed by binning and modifying our data. In the context of the *Quaia* selection function (a measure for the completeness of QSO detections per pixel), we show on the top panel the role of the G -band extinction correction to $G - t$ (our proxy for the radio loudness), and the overall spread of the *Quaia*-VLASS catalogue as a function of this systematic parameter of the input data.

The colour of the data points corresponds to their G -band magnitudes (as shown in Fig. 5). Empty circles mark the average value of $G' - t$ within a given bin of the selection function values, considering the raw G' magnitudes (not corrected for extinction). In contrast, full black circles show the binned average $G - t$ values after extinction correction.

From the comparison to the overall mean $G - t$ value of the whole *Quaia*-VLASS sample (horizontal line), we found that the extinction correction is effective in reducing the deviations between $G - t$ values measured at low vs. high selection function values. The top panel of Fig. 7 demonstrates that most filled circles fall within 1σ of the global mean $G - t$ value for all cross-matches. This result further justifies our use of the extinction-corrected G -band values in subsequent analyses, and

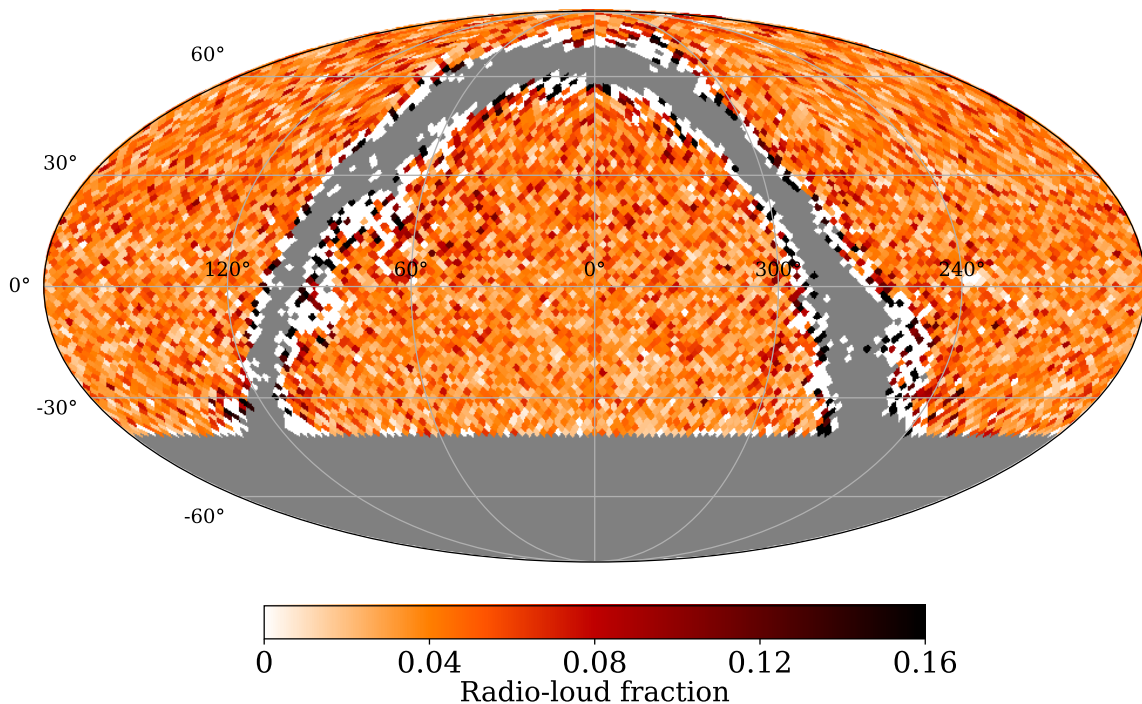


Fig. 8: Radio-loud QSO fraction values in different parts of the sky are shown. We find significant fluctuations near the Milky Way, i.e. where the *Quiaia* catalogue is knowingly less complete (although on average there are no clear biases near the Galactic plane either, see top panel of Fig. 7). In the cleanest areas of the sky, we do not identify any relevant anisotropy in the radio-loud fraction.

it suggests that Galactic dust extinction will not significantly affect our radio-loudness analysis.

3.4. Radio loudness vs. redshift

To perform a further test of systematics, we looked for possible changes in radio loudness as a function of QSO redshift. As shown in Fig. 7 (bottom panel), we observed a moderately significant bias in the average $G-t$ distribution (i.e. in the proxy for radio loudness) at the lowest redshifts ($z < 0.5$). We estimated this statistic for the three G -bins that we considered above, and we found almost identical trends as for the $G < 20.5$ case.

The source of this biased $G-t$ distribution at the low-redshift part of the *Quiaia* QSO catalogue remains unclear. One possibility is that the star-galaxy-QSO separation in the *Gaia-WISE* colour space is less efficient, or the photometric redshifts of the quasars might also be biased at the lowest redshifts where the training set based on Sloan Digital Sky Survey (SDSS) data is less complete. For a detailed explanation, further measurements and statistical probes would be required, which are beyond the scope of this paper.

3.5. Radio-loud fraction across the sky

Looking for possible large-scale spatial patterns on the sky, we created a pixelized map of the radio-loud QSO fraction within each pixel. In Fig. 8, a rather homogeneous distribution is shown across the full observed area, except close to the Galactic plane.

We note that the fluctuations in radio loudness are naturally stronger at low Galactic latitudes, due to sparsity of the QSOs (see the top panel of Fig. 1). For a conservative analysis, future users of our *Quiaia-VLASS* catalogue may apply specific cuts in the *Quiaia* selection function map¹, offering convenient ways of limiting the analyses to the cleanest and most complete parts of the sky.

3.6. Radio-loud fraction vs. absolute magnitude

Additionally, we tested the possible dependence of the radio-loud fraction on the *absolute* magnitudes of the quasars. Following Ivezic et al. (2002), we used the absolute magnitude G_{abs} , which we calculated as

$$G_{\text{abs}} = G + 5 - 5 \cdot \log(d_{\text{lm}}(z)), \quad (5)$$

¹ Publicly available at <https://zenodo.org/records/10403370>

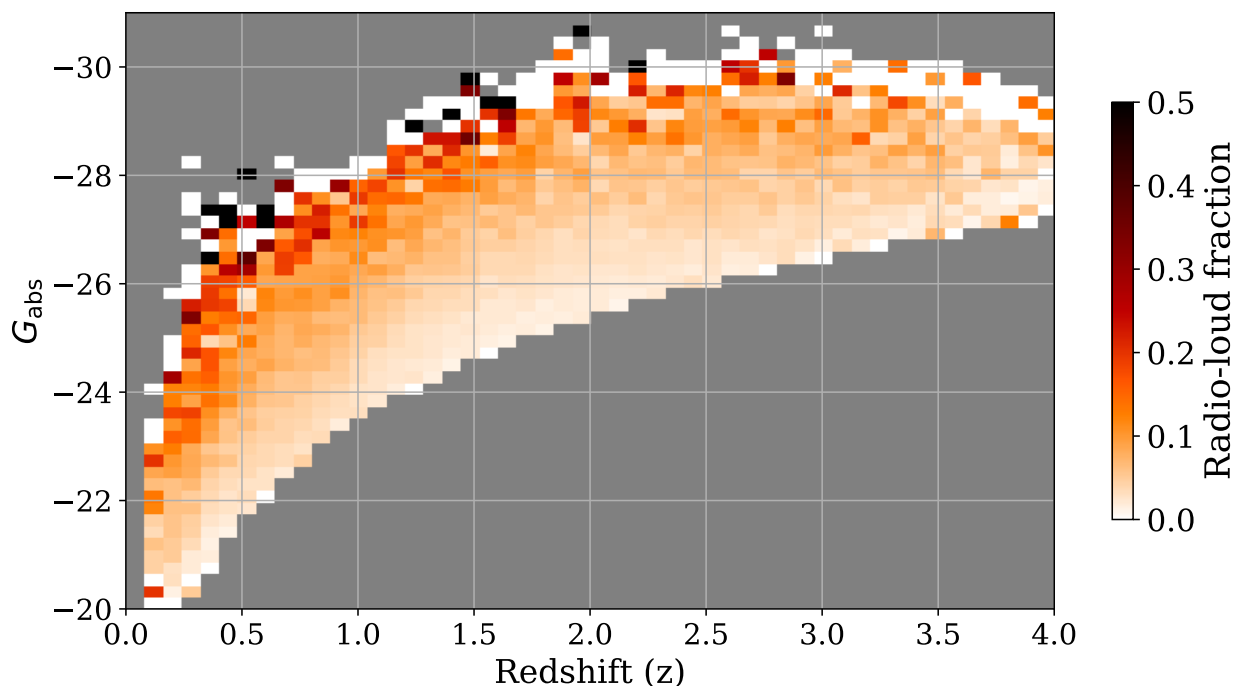


Fig. 9: Radio-loud fraction of *Quaia* sources colour-coded as a function of the absolute magnitude G_{abs} and the redshift z . We observed significant noise due to small-number statistics at the bright-end pixels, leading to strong fluctuations in the radio-loudness fraction.

where $d_{\text{lm}}(z)$ is the luminosity distance² of the object, calculated with *astropy*³.

We highlight here that we consider this as an exploratory test, because the *Quaia* photometric redshifts have a non-negligible uncertainty compared to more ideal spectroscopic redshifts of QSOs. These errors also propagate to our estimation of the luminosity distances, and therefore to the G_{abs} values.

Given the above caveats, our main findings regarding the radio-loud fraction patterns in G_{abs} and redshift bins are illustrated in Fig. 9. Each pixel displays the radio-loud fraction of *Quaia* sources in that bin, using a colour-coding scheme to easily identify any possible trend in the data along either axis.

The figure allows a separate analysis of constant z values in rows against varying G_{abs} values in columns, or vice versa. We found that for a fixed redshift value, radio-loud fraction increases towards brighter G_{abs} bins. Similarly, for a fixed G_{abs} , the binned radio-loud fraction values show a decreasing trend with increasing redshift.

We note that, besides the known redshift errors, our $G_{\text{abs}} - z$ plot in Fig. 9 displays significant noise due to the sparsity of objects in pixels with the most negative G_{abs} values, leading to large fluctuations in radio-loud fractions. Hence we suggest that QSOs falling in these pixels should be flagged or ignored in any subsequent analyses of redshift- and magnitude-dependence of radio-loud fraction that use our *Quaia*–VLASS catalogue.

3.7. Radio-loud vs. radio-quiet source characteristics

In our analysis, we mostly followed Ivezic et al. (2002) and explored if radio-loud and radio-quiet QSOs are statistically consistent with each other, including differently binned subsets. To

this end, they compared the normalized histograms of radio-loud and radio-quiet sources as a function of the i -band absolute magnitude (similar to our Fig. 10). Above all, they identified an excess of radio-quiet QSOs in the faintest bins, followed by a more abundant radio-loud population, and then again more radio-quiet sources at the peak of the distribution.

Ivezic et al. (2002) attributed these features to noise fluctuations and claimed that differences might only be caused by a few dozen sources. In our analysis, we created similar histograms (see the right panel in Fig. 10) using G_{abs} (limited to objects with $G < 18.5$), as opposed to i_{abs} and an $i < 18.5$ cut in previous work. Further, we analyzed more sources with 7,431 radio-loud QSOs at $G < 18.5$, compared to their 280 radio-loud sources at $i < 18.5$. Consequently, our larger data set is expected to help clarify the nature of the excess radio-loud populations in some G_{abs} bins, that were identified as random patterns in previous work (Ivezic et al. 2002).

Considering the brighter $G < 18.5$ subset of our *Quaia*–VLASS quasars, we found that an excess of radio-loud sources does persist at $G_{\text{abs}} \approx -24$, and given the statistical errors in our sample, this pattern certainly reaches several standard deviations in three neighbouring bins (see the right panel in Fig. 10).

On the left side of Fig. 10, we present an analogous histogram for the full *Quaia*–VLASS sample ($G < 20.5$) for a more inclusive analysis. We found that the excess of radio-loud sources persists even in the full sample, albeit in a less pronounced manner. In this larger catalogue, we also noted a similar radio-loud excess for the brightest sources at $-30 < G_{\text{abs}} < -27$. Identifying its origin and exact significance is beyond the scope of this paper, as they might be attributed to yet-unknown systematic effects in the data, or they might be sourced by the *Quaia* photometric redshift errors.

² Assuming a *Planck* Λ CDM cosmology (Planck Collaboration et al. 2020)

³ <https://www.astropy.org/>

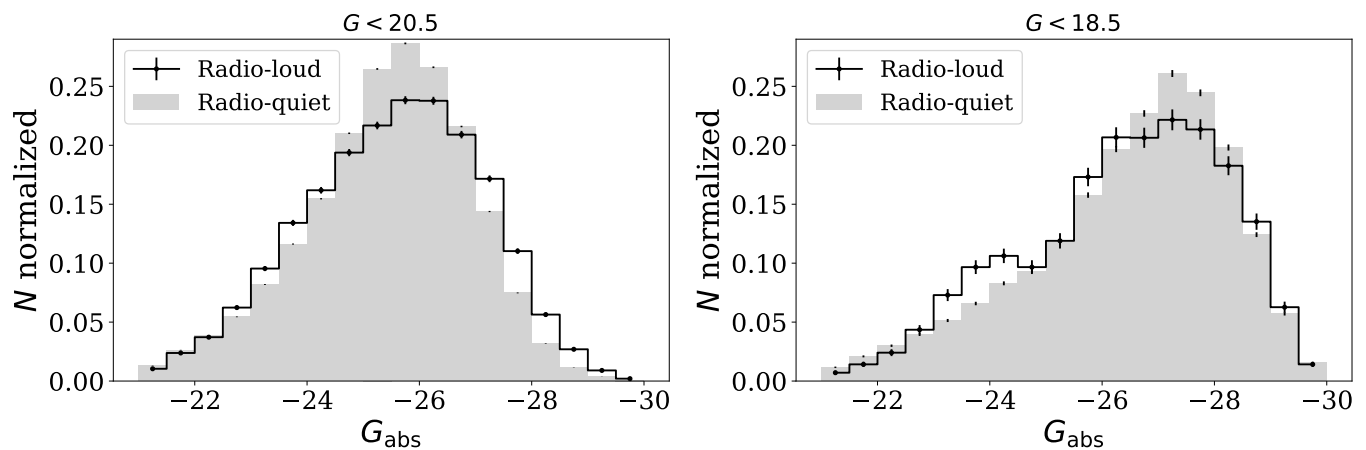


Fig. 10: Normalized histograms of the radio-loud and radio-quiet populations as a function of G_{abs} . On the left, we show the full sample of cross-matches, while on the right a $G < 18.5$ cut is applied.

4. Summary and conclusions

Driven by the availability of modern survey data sets to improve our overall understanding of the astrophysical and cosmological properties of QSOs, we cross-matched the optically selected *Quaia* (*Gaia*+WISE) catalogue of quasars with the VLASS radio sources. In our methodology, we closely followed Ivezic et al. (2002) who also analysed the properties of radio-loud QSOs in a similar context, but using significantly smaller data sets. Our main results are the following:

1. We created a *Quaia*–VLASS catalogue of 43,650 QSOs at declinations $\delta > -40^\circ$ with matched radio counterparts, and we make this new catalogue publicly available for further analyses.
2. We measured the radio loudness as a function of the G apparent magnitude, and found consistent results with Ivezic et al. (2002) considering a similar magnitude limit ($G < 18.5$).
3. We identified weak trends of radio-loudness changes as a function of the *Quaia* completeness and as a function of redshift, both pointing to possible systematic effects as sources.
4. We followed up on the findings by Ivezic et al. (2002) in the context of G_{abs} absolute magnitude statistics, and confirmed the previously seen excess of radio-loud quasars at about $G_{\text{abs}} \approx -24$, for the brightest optical sources ($G < 18.5$).

In summary, here we provided a detailed presentation of the *Quaia*–VLASS catalogue, and performed various statistical analyses in different subsets of the data to spot possible discrepancies or unexpected trends. While our findings already provided new insights on the radio properties of quasars, the upcoming release of the VLASS Epoch3 catalogue will facilitate an even more advanced analysis. With sources much fainter in the radio, we will further explore the dichotomy between radio-loud and radio-quiet sources, as well as possible relations between the positions of the QSOs in the large-scale cosmic web around them, among other potential applications.

Data availability

The *Quaia* quasar catalogue and its mask and selection function are publicly available⁴. The VLASS radio source catalogue is also publicly available⁵, and we will make our cross-matched

Quaia–VLASS data sets, codes and user instructions available publicly⁶.

Acknowledgments

The Large-Scale Structure (LSS) research group at Konkoly Observatory has been supported by a *Lendület* excellence grant by the Hungarian Academy of Sciences (MTA). This project has received funding from the European Union’s Horizon Europe research and innovation programme under the Marie Skłodowska-Curie grant agreement number 101130774. Funding for this project was also available in part through the Hungarian National Research, Development and Innovation Office (NKFIH, grants OTKA NN147550 and K134213). S.F. was supported by the NKFIH excellence grant TKP2021-NKTA-64. L.S.-M was partially supported by the Bulgarian Ministry of Education and Science under Agreement D01-326/04.12.2023. The authors thank Kate Storey-Fisher and the *Quaia* team for their help with the input quasar catalogue.

References

- Arnudova, M. I., Smith, D. J. B., Hardcastle, M. J., et al. 2024, MNRAS, 528, 4547
- Baloković, M., Smolčić, V., Ivezic, Ž., et al. 2012, ApJ, 759, 30
- Blandford, R., Meier, D., & Readhead, A. 2019, ARA&A, 57, 467
- Casagrande, L. & VandenBerg, D. A. 2018, MNRAS, 479, L102
- Charlot, P., Jacobs, C. S., Gordon, D., et al. 2020, A&A, 644, A159
- Delchambre, L., Bailer-Jones, C. A. L., Bellas-Velidis, I., et al. 2023, A&A, 674, A31
- Fabian, A. C. 2012, ARA&A, 50, 455
- Flesch, E. W. 2023, The Open Journal of Astrophysics, 6, 49
- Gaia Collaboration, Bailer-Jones, C. A. L., Teyssier, D., et al. 2023a, A&A, 674, A41
- Gaia Collaboration, Prusti, T., de Bruijne, J. H. J., et al. 2016, A&A, 595, A1
- Gaia Collaboration, Vallenari, A., Brown, A. G. A., et al. 2023b, A&A, 674, A1
- Gordon, Y., Vantghem, A., Sebastian, B., et al. 2023, https://ws.cadc-ccda.hia-ihp.nrc-cnrc.gc.ca/files/vault/cirada/tutorials/CIRADA_VLASS_catalogue_documentation_2023_june.pdf
- Goulding, A. D., Greene, J. E., Setton, D. J., et al. 2023, ApJ, 955, L24
- Gürkan, G., Hardcastle, M. J., Best, P. N., et al. 2019, A&A, 622, A11
- Gurvits, L. I., Kellermann, K. I., & Frey, S. 1999, A&A, 342, 378
- Hardcastle, M. J. & Croston, J. H. 2020, New A Rev., 88, 101539
- Ivezic, Ž., Menou, K., Knapp, G. R., et al. 2002, AJ, 124, 2364

⁶ See <http://konkoly.hu> for information about our data.

⁴ <https://zenodo.org/records/10403370>

⁵ <https://cirada.ca/vlascatalogueq10>

- Kellermann, K. I., Condon, J. J., Kimball, A. E., Perley, R. A., & Ivezić, Ž. 2016, *ApJ*, 831, 168
- Kellermann, K. I., Sramek, R., Schmidt, M., Shaffer, D. B., & Green, R. 1989, *AJ*, 98, 1195
- Kovács, A., Beck, R., Smith, A., et al. 2022, *MNRAS*, 513, 15
- Kreuzinger, M., Baldini, G., Giroletti, M., et al. 2024, *A&A*, 690, A321
- Lacy, M., Baum, S. A., Chandler, C. J., et al. 2020, *PASP*, 132, 035001
- Lang, D. 2014, *AJ*, 147, 108
- Miller, L., Peacock, J. A., & Mead, A. R. G. 1990, *MNRAS*, 244, 207
- Orosz, G. & Frey, S. 2013, *A&A*, 553, A13
- Padovani, P. 2017, *Nature Astronomy*, 1, 0194
- Padovani, P., Alexander, D. M., Assef, R. J., et al. 2017, *A&A Rev.*, 25, 2
- Peacock, J. A., Miller, L., & Longair, M. S. 1986, *MNRAS*, 218, 265
- Piccirilli, G., Fabbian, G., Alonso, D., et al. 2024, *J. Cosmology Astropart. Phys.*, 2024, 012
- Planck Collaboration, Aghanim, N., Akrami, Y., et al. 2020, *A&A*, 641, A6
- Sandage, A. 1965, *ApJ*, 141, 1560
- Schlegel, D. J., Finkbeiner, D. P., & Davis, M. 1998, *ApJ*, 500, 525
- Schmidt, M. 1963, *Nature*, 197, 1040
- Schmidt, M. 1970, *ApJ*, 162, 371
- Sramek, R. A. & Weedman, D. W. 1980, *ApJ*, 238, 435
- Storey-Fisher, K., Hogg, D. W., Rix, H.-W., et al. 2024, *ApJ*, 964, 69
- Strittmatter, P. A., Hill, P., Pauliny-Toth, I. I. K., Steppe, H., & Witzel, A. 1980, *A&A*, 88, L12
- Terashima, Y. & Wilson, A. S. 2003, *ApJ*, 583, 145
- Urry, C. M. & Padovani, P. 1995, *PASP*, 107, 803
- Vermeulen, R. C. & Cohen, M. H. 1994, *ApJ*, 430, 467